HHS Public Access

Author manuscript

Clin Exp Metastasis. Author manuscript; available in PMC 2015 March 06.

Published in final edited form as:

Clin Exp Metastasis. 2014 June ; 31(5): 573–584. doi:10.1007/s10585-014-9651-8.

Development of a realistic in vivo bone metastasis model of human renal cell carcinoma

Maija P. Valta,
Department of Urology, Stanford University School of Medicine, Stanford, CA 94305, USA; Division of Medicine, Turku University Hospital and University of Turku, Turku, Finland

Hongjuan Zhao,
Department of Urology, Stanford University School of Medicine, Stanford, CA 94305, USA

Alexandre Ingels,
Department of Urology, Stanford University School of Medicine, Stanford, CA 94305, USA; Department of Urology, Bicetre Hospital, Paris, France

Alan E. Thong,
Department of Urology, Stanford University School of Medicine, Stanford, CA 94305, USA

Rosalie Nolley,
Department of Urology, Stanford University School of Medicine, Stanford, CA 94305, USA

Matthias Saar, and
Department of Urology, Stanford University School of Medicine, Stanford, CA 94305, USA; Department of Urology and Pediatric Urology, University of Saarland, Homburg/Saar, Germany

Donna M. Peehl
Department of Urology, Stanford University School of Medicine, Stanford, CA 94305, USA

Abstract

About one-third of patients with advanced renal cell carcinoma (RCC) have bone metastases. The incidence of RCC is increasing and bone metastatic RCC merits greater focus. Realistic preclinical bone metastasis models of RCC are lacking, hampering the development of effective therapies. We developed a realistic in vivo bone metastasis model of human RCC by implanting precision-cut tissue slices under the renal capsule of immunodeficient mice. The presence of disseminated cells in bone marrow of tissue slice graft (TSG)-bearing mice was screened by human-specific polymerase chain reaction and confirmed by immunohistology using human-specific antibody. Disseminated tumor cells in bone marrow of TSG-bearing mice derived from three of seven RCC patients were detected as early as 1 month after tissue implantation at a high frequency with close resemblance to parent tumors (e.g., CAIX expression and high vascularity). The metastatic patterns of TSGs correlated with disease progression in patients. In addition, TSGs retained capacity to metastasize to bone at high frequency after serial passaging and cryopreservation.

dpeehl@stanford.edu.

Electronic supplementary material The online version of this article (doi:10.1007/s10585-014-9651-8) contains supplementary material, which is available to authorized users.

Conflict of interests The authors declare that they have no conflict of interests.

Moreover, bone metastases in mice responded to Temsirolimus treatment. Intratibial injections of single cells generated from TSGs showed 100 % engraftment and produced X-ray-visible tumors as early as 3 weeks after cancer cell inoculation. Micro-computed tomography (μCT) and histological analysis revealed osteolytic characteristics of these lesions. Our results demonstrated that orthotopic RCC TSGs have potential to develop bone metastases that respond to standard therapy. This first reported primary RCC bone metastasis model provides a realistic setting to test therapeutics to prevent or treat bone metastases in RCC.

Keywords

Renal cell carcinoma; Tumorgrafts; Bone metastasis; Therapy response

Introduction

Bone is a common site of metastasis in patients with renal cell carcinoma (RCC), affecting one-third of patients with metastatic disease [1, 2]. RCC bone metastases are predominantly osteolytic, cause significant morbidity and are associated with one of the highest rates of skeletal complications of solid tumors [2]. There is growing evidence that the presence of bone metastases in individuals with metastatic RCC is associated with an adverse effect on outcome [3-6]. Bone-targeted treatments using bisphosphonate and denosumab reduce skeletal complications of bone metastatic RCC [7-9] but do not cure the disease or have significant effects on survival. Additionally, a high incidence of osteonecrosis of the jaw limits the therapeutic application of bisphosphonate and denosumab [10]. More effective and less toxic treatments are urgently needed for RCC patients with bone metastases. However, investigations of the impact of therapies on RCC bone metastases are rare because patients with bone-only metastases are often excluded from clinical trials due to the lack of measurable disease by RECIST response criteria. Therefore, it is imperative to develop realistic preclinical models to better understand the biology of RCC bone metastasis and discover effective treatments, especially since the incidence of RCC is increasing [11].

Currently, few preclinical animal models for bone metastatic RCC are available. The published models include intracardiac [12-14], intratibial [13, 15, 16] or tail vein injections [17] of either human 786-0 [12], RBM1 [15,16], SNC12C [13], ACHN [17] cell lines or rat ACI-RCC cells [14] that produced osteolytic or mixed osteoblastic [13] lesions in bones of mice. Of these only 786-0 is purely a clear cell carcinoma of origin, while the others are metastatic (RBM1), less common papillary carcinoma (ACHN), insufficiently defined mixed clear cell and granular cell (SN12C), and moderately differentiated basophilic cell type rat carcinoma (ACI-RCC). Although these models have provided valuable insights into development of RCC bone metastases [13] [15, 16] [18], the value of using cell lines is diminished by long term culture, which allows accumulation of changes during adaptation to growth in vitro and subsequent expansion in the absence of critical components of the tissue microenvironment [19]. Tumors formed by cell lines in mice are often poorly differentiated and likely without resemblance to the tumor from which the cell line was originally derived [20]. In addition, RCC cell lines inoculated orthotopically into mice do not metastasize to bone [14].

The lack of realistic preclinical models, which contributes to the high failure rate of anticancer drug development [21], may be overcome by the use of tumorgrafts derived from fresh specimens of solid tumors, so called “mouse avatars” [22], because of their high predictive power for both patient prognosis and drug response [23-26]. Herein, we report the development and validation of a primary human RCC bone metastasis model using a patient-derived tissue slice graft (TSG) technique recently developed in our lab [27]. This grafting method utilizes precision-cut thin slices of tumor tissue, which allows the generation of large, uniformly sized tumorgraft cohorts from a single tissue core and adequate diffusion of oxygen and nutrients, ensuring a high rate of engraftment. The maintenance of the tumor microenvironment, typically including the survival of human stromal cells, contributes to the authenticity of the model and provides a realistic preclinical setting for therapeutics targeting the microenvironment. This is especially important for RCC as many targeted therapies primarily act on tumor vasculature [28].

We previously showed that TSGs derived from primary RCC tissues maintained appropriate histology, immunophenotype, gene expression, and genetic mutations, and responded to established as well as experimental drug treatments for RCC [27]. In this study, we analyzed and characterized the capacity of primary human RCC cells in TSGs to disseminate and metastasize to bone in mice. We detected bone metastases in TSG-bearing mice by quantitative real-time polymerase chain reaction (qRT-PCR) using human-specific primers and by immunohistochemistry using human-specific antibody. In addition, we examined the capacity of TSGs to metastasize to bone after serial passaging and cryopreservation and determined response of bone metastases to a standard therapy for advanced RCC. Finally, we generated bone tumors in mice by intratibial injection of single cells derived from TSGs.

Materials and methods

Ethics statement

All animal studies were approved by the Stanford Administrative Panel on Laboratory Animal Care (APLAC) and done in compliance with the regulations for animal studies at Stanford University. Primary RCC tissues were obtained immediately after surgery under a protocol approved by the Stanford Institutional Review Board. The participants provided written informed consent to participate in this study.

Tissue acquisition, TSG generation and drug administration

Fresh RCC tissues were obtained from seven patients undergoing radical or partial nephrectomy (clinicopathological features of these cases are summarized in Table 1). A Krumdieck tissue slicer (Alabama Research and Development, Munford, AL) was used to prepare precision-cut tissue slices as previously described [27, 29, 30], with the exception that cores were not embedded in agarose prior to slicing. Briefly, each 8-mm diameter tissue core was sliced at 300-μm. Tissue slices were then implanted under the renal capsules of immunodeficient RAG2$^{-/-}\gamma C^{-/-}$ mice as previously described [27, 29]. One month after implantation, placebo or Temsirolimus (Sigma-Aldrich, St. Louis, MO) was administered by intra-peritoneal injection, once a week, 10 mg/kg/week, as previously described [31].

Cryopreservation of tissue slices

Each fresh tissue slice was submerged in 1 ml of freezing solution [95 % fetal bovine serum (FBS) (Hyclone, Logan, UT) and 5 % DMSO], which has been shown to preserve viability of breast cancer tissues [23], in a 2 ml sterile cryotube. The tubes were then placed in a Nalge Nunc Cryo 1 °C Mr. Frosty Freezing Container (Nalge Nunc International, Rochester, NY) at −70 °C overnight. The tubes were transferred to a liquid nitrogen freezer the next day for long-term storage. Tissues were thawed quickly by agitating the tubes in a 37 °C water bath and rinsed 2× with HEPES-buffered saline (HBS) before implantation into mice.

Immunohistochemistry and TRAP-staining

Immunohistochemistry was performed as previously described [29], except that tibia and femur were fixed in 10 % formalin for 2 days, incubated in 14 % EDTA for 15 days, paraffin-embedded and sectioned at 5-m throughout. The sources and dilutions of antibodies used in this study are listed in Supplementary Table 1. Tartrate-resistant acid phosphatase (TRAP) staining for detecting osteoclasts was performed as previously described [32].

Preparation of single cell population

Mice bearing TSGs were sacrificed and TSGs were dissected free of surrounding mouse kidney. TSGs were placed in the Krumdieck tissue slicer and cut at 300-μm. Sequential sections were collected and alternating sections were frozen for histological analysis. Only tissue sections adjacent to frozen sections free of necrosis or cystic structures were used to generate single cells. Tissue slices were minced with scissors and then digested in DMEM/F12 + GlutaMAX-I™ (Invitrogen, Carlsbad, CA) supplemented with 10 % FBS and 200 U/ml Collagenase type I (Sigma-Aldrich), 1 U/ml DNase I (Invitrogen), 2 μM Y27632 (Sigma-Aldrich), and antibiotics for a total of 30 min at 37° C. The mixture was pipetted up and down every 10 min. The digested tissue was passed through a 40-μm cell filter (BD Biosciences, Bedford, MA) and the cells that passed through the filter were collected. At this point, cells were either immediately inoculated intratibially into mice or cryopreserved in DMEM/F12 + GlutaMAX-I™ supplemented with 10 % FBS and 5 μg/ml holo-transferrin (Sigma-Aldrich), 10 % DMSO and antibiotics. Prior to inoculation into mice, the cells were suspended at a concentration of 5×10^5 live cells/20 μl of HBS and kept on ice until inoculation.

Intratibial injections

Twelve-week-old RAG2$^{-/-}\gamma C^{-/-}$ mice were used for the intratibial injection of single RCC cells generated from TSGs, as previously described [33]. Briefly, 20 μl of cell suspension or HBS were inoculated into the right or left tibiae, respectively. A 28-gauge needle was inserted ~5-mm deep into the proximal end of the tibia using a drilling motion. To verify the correct position of the needle inside the tibial cavity, the tibia and the needle were then X-rayed with Progeny Dental VetVision DC Model 30-A1027 X-ray (65 kV, 0.032 s, Midmark Corp, Versailles, OH). If the position was correct, the needle was removed, and another needle was inserted and 20 μl of cell suspension or HBS were slowly inoculated into tibia. The tibiae were X-rayed weekly for signs of tumor growth. Bones were also analysed with micro-computed tomography (μCT) and immunohistochemistry.

Extraction of RNA from bone marrow and quantitative real-time PCR (qRT-PCR)

Bones were rinsed in sterile HBS, placed on a sterile culture dish in a ventilated hood and cut open with a surgical knife along the longitudinal axis. Using sterile instruments, marrow was extracted and immersed in 100 μl of RNA-Later (Qiagen, Germantown, MD). Equipment was changed between samples to avoid contamination. RNA extraction was performed using an AllPrep DNA/RNA/Protein Mini Kit (Qiagen). The quality of RNA was determined by spectrophotometry and on 1 % agarose gels. qRT-PCR was performed as previously described [34]. Primer sequences for human-specific and universal GAPDH are listed in Supplementary Table 2. To determine the sensitivity of the assay, 100 μl of mouse blood was spiked with 10, 100 or 1,000 human prostate cancer LNCaP cells and qRT-PCR was performed using RNA samples isolated from the mixtures. The Ct values for the samples containing 10, 100, and 1,000 LNCaP cells were on average 37, 30, and 25, respectively. No signal was detected in mouse blood in which no LNCaP cells were spiked. A Ct value of 37 was used to define the limit of detection.

μCT analysis

μCT was performed in vivo on a Siemens ImTek Micro-CAT II microtomograph (Siemens, Munich, Germany) at Stanford Center for Innovation in In-Vivo Imaging. Image analysis and 3D representations were conducted with GEHC Micro View Version MicroView Analysis +2.2 (GE Healthcare, Wauwatosa, WI).

Statistical analysis

Student's *t* test was used for two-arm experiments (Excel Stats). A $p < 0.05$ was considered significant.

Results

Primary RCC has potential to metastasize to bone in TSG model

Fresh primary RCC specimens were obtained from 7 patients (Table 1) after nephrectomy, precision-cut and implanted under the renal capsule of immunodeficient mice. Six of the 7 cases were clear cell RCC (ccRCC) and one case was diagnosed as chromophobe RCC. Only one patient (case 6) had undergone therapy prior to nephrectomy. The engraftment rate, time after implantation and average TSG weight at sacrifice for each case are listed in Supplementary Table S3. Only mice with engrafted TSGs were used in this study. Bone marrow from left hind limbs was collected at sacrifice for qRT-PCR analysis, taking high precautions against contamination by human cells. Human GAPDH transcripts were detected in marrow of mice bearing TSGs from 3 of the 7 RCC cases by qRT-PCR using human-specific GAPDH primers. The level of human-specific GAPDH was normalized to the total GAPDH detected by a universal primer pair that recognizes both human and mouse GAPDH in each sample. The limit of detection was determined by spiking mouse blood with human cells (see Methods). The frequency of detection of human GAPDH was 74 % for case 1 (23 of 31 mice), 75 % for case 4 (3 of 4 mice) and 14 % for case 7 (1 of 7 mice) (Table 1). No human GAPDH transcripts were detected in bone marrows from the rest of TSG-bearing mice or mice not implanted with TSGs (n = 6, results not shown).

We next analysed left hind limb bones for metastases by histological methods. Specifically, we determined expression of Ku70 by immunohistochemistry using a human-specific antibody [35]. As shown in Fig. 1, bone metastases from case 1 TSG-bearing mice showed a ccRCC-like histology (Fig. 1a). Eight of 14 (57 %) mice bearing TSGs from case 1 that carried human GAPDH transcripts in the bone marrow also had Ku70- positive cells in the bone (Fig. 1b; Table 1), while no Ku70-positive cells were detected in the control bone (Fig. 1c). We did not analyze histological bone metastases from case 4 due to lack of samples. Bone samples of two mice for case 7 were negative for Ku70, including the one in which human GAPDH transcript was detected in the bone marrow by qRT-PCR. This may be explained by a low number of RCC cells in the bone marrow that is below the detection limit of immunohistochemistry, rather than a false positive qRT-PCR assay, because bone marrow samples from 6 mice not implanted with TSGs were all negative for human GAPDH by qRT-PCR. Altogether, these results demonstrated that TSGs derived from primary RCCs have the potential to metastasize to the bone in mice.

Mice bearing primary RCC from cases 1 and 2 also developed soft tissue metastases (Table 1). Interestingly, clinical follow-up of these patients revealed that patients 1, 2 and 4 had subsequently relapsed with metastatic disease at 6 months after nephrectomy (Table 1). Case 1 had soft tissue metastases in both patient and TSG-bearing mice, while bone metastases were observed in mice but not the patient at the time of follow-up. Case 2 had soft tissue metastases but not bone metastases in both TSG-bearing mice and the patient. Case 4 had bone metastases but not soft tissue metastases in both TSG-bearing mice and the patient. Case 6 had soft tissue metastases before surgery and no gross metastases were detected in TSG-bearing mice, possibly because the pre-operative treatment eliminated tumor cells most likely to metastasize. However, human GAPDH transcripts were detected by qRT-PCR in liver tissues of TSG-bearing mice, indicating dissemination of RCC cells from TSGs to the liver (data not shown). We did not observe distant metastases in case 5 TSG-bearing mice although patient 5 presented with ipsilateral adrenal metastasis. Perhaps the latency of metastasis for this case is longer than the time period examined in this study. Alternatively, metastases may be present in the adrenal glands of the TSG-bearing mice, which were not examined in this study. Nonetheless, these results demonstrated that the metastatic patterns in TSG-bearing mice largely correlated with those in patients.

Immunophenotype of RCC bone metastases in TSG model

Bone metastases from case 1 TSG-bearing mice showed strong staining for CAIX, a typical ccRCC marker (Fig. 1d), while no CAIX-positive cells were detected in control bone (Fig. 1e). Analysis of tumor-bone interface revealed strong activity of osteoclasts as shown by TRAP-staining (Fig. 1f). Endothelial cell-specific CD31 staining revealed a rich vascularization of the metastases (Fig. 1g). Finally, strong Ki67 staining was observed in a majority of cells in the bone metastases, indicating highly proliferating tumor cells (Fig. 1h). These results suggest that RCC bone metastases in the TSG model are osteolytic, i.e., able to activate osteoclasts, and highly proliferative.

TSGs retain capacity to metastasize to bone at high frequency after serial passaging

TSGs derived from case 1 primary RCC were maintained in mice by serial passaging up to 10 times, the highest passage examined. All passaged TSGs retained metastatic capacity to bone at a frequency of 30–100 % as determined by qRT-PCR of human-specific GADPH (Fig. 2a). The ratio of human-specific GAPDH to universal GAPDH was used as a readout of tumor burden in the bone. Mice that were found to have histological bone metastases on the contralateral side had higher tumor burden in the bone by qRT-PCR than those without histological bone metastases (Fig. 2b); however, the difference did not reach statistical significance ($p = 0.30$). These results demonstrated that TSGs retain capacity to metastasize to bone at high frequency after serial passaging.

TSGs retain viability and capacity to metastasize to bone after cryopreservation

TSGs at passages 8–10 from case 1 were either precision-cut or minced, then cryopreserved for several weeks. After thawing, tissues were immediately implanted under the renal capsules of immunodeficient mice. Average engraftment rate from 3 different experiments was 84 % (Table 2), slightly lower than the engraftment rate of TSGs derived from fresh tissues (90–100 %) (Supplementary Table S3). When precision-cut slices were used, TSGs derived from cryopreserved tissues reached similar sizes in the same growth period as TSGs derived from fresh tissues (Tables 2, S3). Cryopreserved minced tissues formed smaller tumors (Table 2); however, the difference was not statistically significant. TSGs derived from cryopreserved tissues displayed similar immunophenotypes including Ku70 and CAIX expression (Fig. 3a-f). Finally, human-specific GAPDH transcripts were detected in the bones of mice bearing TSGs derived from cryopreserved tissues (Table 2). Immunohistochemistry revealed Ku70-expressing cells in the bone and soft tissues of mice bearing TSGs derived from cryopreserved tissues at all passages (Table 2; Fig. 3g–l). These results demonstrated that TSGs retained viability and capacity to metastasize to bone and soft tissues after cryopreservation.

Bone metastases in TSG model responded to standard anti-cancer therapy

To determine whether bone metastases in our TSG model respond to anti-cancer therapy, we randomized mice bearing case 1 TSGs at passage 6 into control and treated groups. The treated group received Temsirolimus, an FDA-approved mTOR inhibitor for treatment of advanced RCC, via intraperitoneal injection, and the placebo group received only vehicle for the same time periods. Treatment started 4 weeks after TSG implantation and continued until sacrifice at 5.5 or 8.5 weeks, and tumor burden in bone was assessed using the ratio of human-specific GAPDH to total GAPDH level in the bone marrow. Bone micrometastasis burden increased from week 5.5 to 8.5 in both the control and treated groups (Fig. 4). Temsirolimus significantly reduced bone micrometastasis after 4.5 but not 1.5 weeks of treatment ($p = 0.025$) (Fig. 4). These results demonstrated that bone metastases in our TSG model responded to a standard therapy for advanced RCC.

RCC cells derived from TSGs induce bone osteolysis in mice similar to human primary RCC

Bone metastatic RCC in human is typically osteolytic, causing a high rate of skeletal-related events [36]. We examined the osteoclastic potential of RCC cells derived from case 1 TSGs at passage 6 in mice. Precision-cut slices of case 1 TSGs were mostly composed of human RCC cells as shown by histology and Ku70 expression (Fig. 5a-c). TSGs were digested into single cells and injected into tibiae of mice, as confirmed by X-ray (Fig. 5i). For comparison, HBS was injected into contralateral tibiae as a control. We found evident osteolysis in cortical bone at week 4 (Fig. 5d–e) and week 6 (Fig. 5f–g) by μCT imaging in all RCC cell-injected tibiae. Quantitation of bone volume at proximal tibial epiphyseal regions showed an overall reduction in bone volume of primary RCC cell-injected tibiae compared to control tibiae 6 weeks after injection (Fig. 5h). Consecutive X-ray images revealed an advancing osteolytic reaction at week 3 (Fig. 5k) and week 5 (Fig. 5l), which was not present before injection (Fig. 5j). Histological cross-sections of RCC cell-injected tibiae confirmed nearly complete destruction of trabecular bone (Fig. 5m) compared to the contralateral HBS-injected side (Fig. 5n). Finally, single cells derived from case 1 TSGs that had been cryopreserved for several weeks engrafted at a rate of 100 % after intratibial injection (Table 3) as demonstrated by strong Ku70 and Ki67 immunohistochemical staining (data not shown). In addition, strong osteolytic reactions induced by the injected cells, similar to non-cryopreserved fresh cells, were revealed by μCT imaging compared to contralateral tibiae (Table 3), confirming the engraftment of the cells.

TRAP staining showed high osteoclastic activity at sites where injected RCC cells formed intratibial tumors that invaded outside cortical bone (Fig. 6a). The intratibial tumors demonstrated similar histology to TSGs (H&E, Fig. 6b) and consisted of Ku70-positive (Fig. 6c) and CAIX-positive (Fig. 6d) human cells. Many areas showed highly proliferating cells (Ki67 immunohistochemical staining, Fig. 6e) with rich neovasculature (Fig. 6f). These results demonstrated that single cells derived from RCC TSGs induced bone osteolysis in mice similar to human primary RCC.

Discussion

We developed a novel preclinical model of bone metastasis for primary RCC that resembles the human disease. Three of seven TSG cohorts derived from fresh primary RCC specimens developed metastases to bone and/or soft tissues at clinically relevant sites (lung, liver) in mice. The metastatic patterns were largely correlated with those observed in patients from whom the TSGs were derived. Moreover, we observed close resemblance of bone metastases derived from TSGs to parent tumors in immunophenotypic characteristics. Finally, these bone metastases responded to a standard therapy for advanced RCC and induced bone osteolysis in mice similar to human metastatic RCC. To our knowledge, these are the first reported models of primary RCC metastasis to bone, which will serve as a powerful tool in understanding the biology of bone metastases and the discovery of effective therapies for bone metastatic RCC.

Bone metastases are rare in animal models of solid tumors, including those with high incidence of bone metastases in patients such as breast and prostate cancer. In RCC, bone is

the second most common metastatic site after lung [1], yet, in a recent study investigating metastatic capacity of orthotopic RCC xenografts, only spontaneous metastases to soft tissues, but not to bone, were observed [37]. This is in part due to the difficulty of achieving gross metastases in animal models with the primary tumor in place, because mice have to be sacrificed when primary tumors attain a certain volume. One strategy to overcome this problem is to resect primary tumors to allow the growth of metastatic cells. Using this strategy, DeRose et al. [23] observed metastases of breast cancers to multiple sites including the bone after removing the primary tumors in the fat pad. We have attempted cytoreductive nephrectomy in our TSG models, however, it is technically challenging.

We detected bone metastases in TSG-bearing mice using two methods: qRT-PCR quantification of human-specific GAPDH, and immunohistochemistry using human-specific Ku70 antibody and CAIX, specific for RCC. No signals were observed from mice without TSGs, lessening the possibility that human cell contamination occurred in the procedures. We observed high frequency of bone metastases in some RCC cases. Tumor cells from approximately 75 % of TSGs derived from case 1 and case 4 spread to bones in mice based on qRT-PCR of human GAPDH, and 57 % of animals with positive qRT-PCR from case 1 were found to have immunohistochemically confirmed bone metastases on the contralateral hind limb. It is expected that the sensitivity of qRT-PCR will be higher compared to immunohistochemistry. We predict that mice that are negative for bone metastases by immunohistochemistry but positive by qRT-PCR would eventually develop microscopic bone lesions. The relatively high frequency of bone metastases that we observed may be attributed to the use of $RAG2^{-/-}\gamma C^{-/-}$ mice as the host of TSGs in our study. These mice lack active B and T cells as well as NK cells [38] and permit superior engraftment of human tissues/cells compared to other strains of mice [39]. In addition, use of precision-cut tissue slices which leads to high engraftment rate of TSGs may also contribute to the high frequency of bone metastases [27]. Finally, the presence of stromal elements in TSGs may be vital for bone metastatic dissemination. An et al. demonstrated that tissue architecture of the implanted tumor tissue in an orthotopic RCC model played an important role in the initiation of primary tumor growth, invasion, and distant metastasis [40]. A more recent study by Zhang et al. [41] illustrated that primary breast tumor stroma may dictate the bone metastasis phenotype, both supporting a critical role of tumor stroma in metastasis.

Interestingly, follow-up at 6 months after resection of primary patient tumors revealed similar metastatic patterns in patients compared to derivative TSGs in mice. For example, tumors in patient 2 and patient 4 showed the same metastatic patterns as corresponding TSGs in mice, indicating that TSGs are predictive of metastatic disease and may provide prognostic information for RCC management. Chromophobe RCC (patient 4) typically has a more favorable prognosis but metastasizes to bone with similar frequency compared to other subtypes [42]. A growing inventory of new agents has been discovered that may improve the clinical outcome of advanced RCC including compounds targeting the vascular endothelial growth factor (VEGF) axis and those targeting mTOR [43-46]. However, clinical trials evaluating such candidate compounds require a large number of patients, are expensive and time-consuming, and expose patients to certain risks. Moreover, bone metastases are not considered to be measurable by RECIST criteria and in fact are difficult lesions to assess by

imaging, as they tend to change in radiological appearance rather than in size. Accordingly, little is known about the response of bone metastases to these new targeted therapies. The TSG model of RCC bone metastasis provides a much-needed pre-clinical screening platform that can be used to rapidly narrow down the number of agents or regimens for further investigation. The authenticity of the model in recapitulating the features of the parent tumors increases confidence in the likelihood of similar drug responses in humans. In addition, our study demonstrates the feasibility of generating a relatively large number of bone metastases from the same RCC specimen with similar cell composition and histology among control and experimental samples in an in vivo setting. These advantages of our model ensure its potential as a novel platform to better understand the mechanisms of bone metastases in RCC and greatly accelerate the discovery of effective therapies.

As proof-of-principle, we tested the effects of Temsirolimus, an FDA-approved mTOR inhibitor for treatment-naïve, poor prognosis metastatic RCC [47], on bone metastases in mice carrying case 1 TSGs. Temsirolimus significantly reduced human GAPDH levels in bone marrow of TSG-bearing mice ($p = 0.025$), suggesting a decrease in bone metastasis. Our studies were not designed to distinguish whether the decrease was due to reduced seeding of disseminated cells from the primary tumor, and hence, the main effect being on the primary tumor, or to inhibition of growth of the cells in the bone. Previous studies have shown that Temsirolimus suppresses osteoclast formation and osteolytic bone destruction associated with invasion of oral squamous cell carcinoma in vivo [48]. In addition, Rapamycin, an analog of Temsirolimus, has been shown to reduce osteolytic bone metastasis in a breast cancer mouse model [49]. Our results are in concordance with these findings and the first to show an effect of an mTOR inhibitor on RCC bone metastasis. Further studies are necessary to confirm these findings in a large number of RCC cases.

Our TSG bone metastasis model for RCC is versatile in two ways. First, TSGs retained viability and capacity to metastasize to bone after cryopreservation. This will allow biobanking of primary RCC tissues, which can be used to generate TSGs that still metastasize to the bone and permit testing of therapeutic agents in case of later metastatic relapse in patients. The knowledge of drug efficacies in the individualized TSG bone metastasis model can then guide the selection of the optimal treatment for a particular patient. Such personalized treatment could greatly improve patient outcome and quality of life. Second, bone tumors can be generated from RCC cells derived from TSGs, which induce bone osteolysis in mice similar to human primary RCC. This will allow rapid generation of bone lesions for high-throughput drug testing, which is particularly important for patients with metastatic disease who are in need of treatment decisions in a timely manner. Altogether, this model offers a unique opportunity to advance our knowledge of not only the biology but also the treatment strategy of RCC bone metastasis.

Supplementary Material

Refer to Web version on PubMed Central for supplementary material.

Acknowledgments

This work was supported by funds from the Department of Urology, Instrumentarium Science Foundation (MPV), Finnish Medical Foundation (MPV), Finnish Cultural Foundation (MPV) and South-Western Cancer Foundation of Finland (MPV), Association Française d'Urologie (AI), and the Ferdinand Eisenberger Grant of the German Society of Urology ID SaM1/FE-11 (MS). The funding institutions did not have any role in the design, collection, analysis, and interpretation of data, in the writing of the manuscript; or in the decision to submit the manuscript for publication. The personnel at Pharmatest Services Ltd. (Turku, Finland) are thanked for TRAP staining.

Abbreviations

CAIX	Carbonic anhydrase IX
CT	Computed tomography
FBS	Fetal bovine serum
HBS	HEPES-buffered saline
qRT-PCR	Quantitative real-time PCR
RCC	Renal cell carcinoma
TRAP	Tartrate-resistant acid phosphatase
TSG	Tissue slice graft

References

1. Bianchi M, Sun M, Jeldres C, Shariat SF, Trinh QD, Briganti A, Tian Z, Schmitges J, Graefen M, Perrotte P, Menon M, Montorsi F, Karakiewicz PI. Distribution of metastatic sites in renal cell carcinoma: a population-based analysis. Ann Oncol. 2012; 23(4):973–980. [PubMed: 21890909]
2. Woodward E, Jagdev S, McParland L, Clark K, Gregory W, Newsham A, Rogerson S, Hayward K, Selby P, Brown J. Skeletal complications and survival in renal cancer patients with bone metastases. Bone. 2011; 48(1):160–166. [PubMed: 20854942]
3. McKay RR, Kroeger N, Xie W, Lee JL, Knox JJ, Bjarnason GA, Mackenzie MJ, Wood L, Srinivas S, Vaishampayan UN, Rha SY, Pal SK, Donskov F, Tantravahi SK, Rini BI, Heng DY, Choueiri TK. Impact of bone and liver metastases on patients with renal cell carcinoma treated with targeted therapy. Eur Urol. 2013; 65(3):577–584. [PubMed: 23962746]
4. Molina AM, Jia X, Feldman DR, Hsieh JJ, Ginsberg MS, Velasco S, Patil S, Motzer RJ. Long-term response to sunitinib therapy for metastatic renal cell carcinoma. Clin Genitourin Cancer. 2013; 11(3):297–302. [PubMed: 23707221]
5. Shinohara N, Nonomura K, Abe T, Maruyama S, Kamai T, Takahashi M, Tatsugami K, Yokoi S, Deguchi T, Kanayama H, Oba K, Naito S. A new prognostic classification for overall survival in Asian patients with previously untreated metastatic renal cell carcinoma. Cancer Sci. 2012; 103(9): 1695–1700. [PubMed: 22642767]
6. Naito S, Yamamoto N, Takayama T, Muramoto M, Shinohara N, Nishiyama K, Takahashi A, Maruyama R, Saika T, Hoshi S, Nagao K, Yamamoto S, Sugimura I, Uemura H, Koga S, Takahashi M, Ito F, Ozono S, Terachi T, Tomita Y. Prognosis of Japanese metastatic renal cell carcinoma patients in the cytokine era: a cooperative group report of 1463 patients. Eur Urol. 2010; 57(2):317–325. [PubMed: 19136199]
7. Keizman D, Ish-Shalom M, Pili R, Hammers H, Eisenberger MA, Sinibaldi V, Boursi B, Maimon N, Gottfried M, Hayat H, Peer A, Kovel S, Sella A, Berger R, Carducci MA. Bisphosphonates combined with sunitinib may improve the response rate, progression free survival and overall survival of patients with bone metastases from renal cell carcinoma. Eur J Cancer. 2012; 48(7): 1031–1037. [PubMed: 22409947]

8. Lipton A, Colombo-Berra A, Bukowski RM, Rosen L, Zheng M, Urbanowitz G. Skeletal complications in patients with bone metastases from renal cell carcinoma and therapeutic benefits of zoledronic acid. Clin Cancer Res. 2004; 10(18 Pt 2):6397S–6403S. [PubMed: 15448038]

9. Henry DH, Costa L, Goldwasser F, Hirsh V, Hungria V, Prausova J, Scagliotti GV, Sleeboom H, Spencer A, Vadhan-Raj S, von Moos R, Willenbacher W, Woll PJ, Wang J, Jiang Q, Jun S, Dansey R, Yeh H. Randomized, double-blind study of denosumab versus zoledronic acid in the treatment of bone metastases in patients with advanced cancer (excluding breast and prostate cancer) or multiple myeloma. J Clin Oncol. 2011; 29(9):1125–1132. [PubMed: 21343556]

10. Beuselinck B, Wolter P, Karadimou A, Elaidi R, Dumez H, Rogiers A, Van Cann T, Willems L, Body JJ, Berkers J, Van Poppel H, Lerut E, Debruyne P, Paridaens R, Schoffski P. Concomitant oral tyrosine kinase inhibitors and bisphosphonates in advanced renal cell carcinoma with bone metastases. Br J Cancer. 2012; 107(10):1665–1671. [PubMed: 23132391]

11. Howlader, N.; Noone, AM.; Krapcho, M.; Garshell, J.; Neyman, N.; Altekruse, SF.; Kosary, CL.; Yu, M.; Ruhl, J.; Tatalovich, Z.; Cho, H.; Mariotto, A.; Lewis, Chen HS.; Feuer, EJ.; KA, C. SEER Cancer Statistics Review, 1975-2010. National Cancer Institute; Bethesda: 2012.

12. Strube A, Stepina E, Mumberg D, Scholz A, Hauff P, Kakonen SM. Characterization of a new renal cell carcinoma bone metastasis mouse model. Clin Exp Metastasis. 2010; 27(5):319–330. [PubMed: 20443133]

13. Josson S, Nomura T, Lin JT, Huang WC, Wu D, Zhau HE, Zayzafoon M, Weizmann MN, Gururajan M, Chung LW. β2-microglobulin induces epithelial to mesenchymal transition and confers cancer lethality and bone metastasis in human cancer cells. Cancer Res. 2011; 71(7):2600–2610. [PubMed: 21427356]

14. Kobayashi M, Morita T, Chun NA, Matsui A, Takahashi M, Murakami T. Effect of host immunity on metastatic potential in renal cell carcinoma: the assessment of optimal in vivo models to study metastatic behavior of renal cancer cells. Tumour Biol. 2012; 33(2):551–559. [PubMed: 22219032]

15. Weber K, Doucet M, Kominsky S. Renal cell carcinoma bone metastasis—elucidating the molecular targets. Cancer Metastasis Rev. 2007; 26(3-4):691–704. [PubMed: 17768599]

16. Weber KL, Pathak S, Multani AS, Price JE. Characterization of a renal cell carcinoma cell line derived from a human one metastasis and establishment of an experimental nude mouse model. J Urol. 2002; 168(2):774–779. [PubMed: 12131367]

17. Wang J, Chen A, Yang C, Zeng H, Qi J, Guo FJ. A bone-seeking clone exhibits different biological properties from the ACHN parental human renal cell carcinoma in vivo and in vitro. Oncol Rep. 2012; 27(4):1104–1110. [PubMed: 22139406]

18. Maita S, Yuasa T, Tsuchiya N, Mitobe Y, Narita S, Horikawa Y, Hatake K, Fukui I, Kimura S, Maekawa T, Habuchi T. Antitumor effect of sunitinib against skeletal metastatic renal cell carcinoma through inhibition of osteoclast function. Int J Cancer. 2012; 130(3):677–684. [PubMed: 21387300]

19. Peterson JK, Houghton PJ. Integrating pharmacology and in vivo cancer models in preclinical and clinical drug development. Eur J Cancer. 2004; 40(6):837–844. [PubMed: 15120039]

20. Sausville EA, Burger AM. Contributions of human tumor xenografts to anticancer drug development. Cancer Res. 2006; 66(7):3351–3354. [PubMed: 16585151]

21. Ocana A, Pandiella A, Siu LL, Tannock IF. Preclinical development of molecular-targeted agents for cancer. Nat Rev Clin Oncol. 2011; 8(4):200–209. [PubMed: 21135887]

22. Dennis C. Mouse ‘avatars’ could aid pancreatic cancer therapy. Nat News. 2012 doi:10.1038/nature.2012.10259.

23. DeRose YS, Wang G, Lin YC, Bernard PS, Buys SS, Ebbert MT, Factor R, Matsen C, Milash BA, Nelson E, Neumayer L, Randall RL, Stijleman IJ, Welm BE, Welm AL. Tumor grafts derived from women with breast cancer authentically reflect tumor pathology, growth, metastasis and disease outcomes. Nat Med. 2011; 17(11):1514–1520. [PubMed: 22019887]

24. Garber K. Personal mouse colonies give hope for pancreatic cancer patients. J Natl Cancer Inst. 2007; 99(2):105–107. [PubMed: 17227991]

25. Garber K. From human to mouse and back: ‘tumorgraft’ models surge in popularity. J Natl Cancer Inst. 2009; 101(1):6–8. [PubMed: 19116380]

26. Hidalgo M, Bruckheimer E, Rajeshkumar NV, Garrido-Laguna I, De Oliveira E, Rubio-Viqueira B, Strawn S, Wick MJ, Martell J, Sidransky D. A pilot clinical study of treatment guided by personalized tumorgrafts in patients with advanced cancer. Mol Cancer Ther. 2011; 10(8):1311–1316. [PubMed: 21673092]
27. Thong AE, Zhao H, Ingels A, Valta MP, Nolley R, Santos J, Young SR, Peehl DM. Tissue slice grafts of human renal cell carcinoma: An authentic preclinical model with high engraftment rate and metastatic potential. Urol Oncol. 2013; 32(1):43.e23–43.e30. [PubMed: 23911681]
28. Huang D, Ding Y, Li Y, Luo WM, Zhang ZF, Snider J, Vandenbeldt K, Qian CN, Teh BT. Sunitinib acts primarily on tumor endothelium rather than tumor cells to inhibit the growth of renal cell carcinoma. Cancer Res. 2010; 70(3):1053–1062. [PubMed: 20103629]
29. Zhao H, Nolley R, Chen Z, Peehl DM. Tissue slice grafts: an in vivo model of human prostate androgen signaling. Am J Pathol. 2010; 177(1):229–239. [PubMed: 20472887]
30. Fisher RL, Vickers AE. Preparation and culture of precision-cut organ slices from human and animal. Xenobiotica; the fate of foreign compounds in biological systems. 2013; 43(1):8–14.
31. Ingels A, Zhao H, Thong A, Saar M, Valta M, Nolley R, Santos J, Peehl DM. Pre-clinical trial of a new dual mTOR inhibitor INK128 for renal cell carcinoma. Int J Cancer. 2013; 134(10):2322–2329. [PubMed: 24243565]
32. Hughes DE, Wright KR, Uy HL, Sasaki A, Yoneda T, Roodman GD, Mundy GR, Boyce BF. Bisphosphonates promote apoptosis in murine osteoclasts in vitro and in vivo. J Bone Miner Res. 1995; 10(10):1478, 1487. [PubMed: 8686503]
33. Valta MP, Tuomela J, Bjartell A, Valve E, Vaananen HK, Harkonen P. FGF-8 is involved in bone metastasis of prostate cancer. Int J Cancer. 2008; 123(1):22–31. [PubMed: 18386787]
34. Zhao H, Nolley R, Chen Z, Reese SW, Peehl DM. Inhibition of monoamine oxidase A promotes secretory differentiation in basal prostatic epithelial cells. Differentiation. 2008; 76(7):820–830. [PubMed: 18248494]
35. Wang J, Chou CH, Blankson J, Satoh M, Knuth MW, Eisenberg RA, Pisetsky DS, Reeves WH. Murine monoclonal anti-bodies specific for conserved and non-conserved antigenic determinants of the human and murine Ku autoantigens. Mol Biol Rep. 1993; 18(1):15–28. [PubMed: 7694076]
36. Saylor PJ, Armstrong AJ, Fizazi K, Freedland S, Saad F, Smith MR, Tombal B, Pienta K. New and emerging therapies for bone metastases in genitourinary cancers. Eur Urol. 2013; 63(2):309–320. [PubMed: 23201471]
37. Grisanzio C, Seeley A, Chang M, Collins M, Di Napoli A, Cheng SC, Percy A, Beroukhim R, Signoretti S. Orthotopic xenografts of RCC retain histological, immunophenotypic and genetic features of tumours in patients. J Pathol. 2011; 225(2):212–221. [PubMed: 21710693]
38. van Rijn RS, Simonetti ER, Hagenbeek A, Hogenes MC, de Weger RA, Canninga-van Dijk MR, Weijer K, Spits H, Storm G, van Bloois L, Rijkers G, Martens AC, Ebeling SB. A new xenograft model for graft-versus-host disease by intravenous transfer of human peripheral blood mononuclear cells in RAG2−/− gammac−/− double-mutant mice. Blood. 2003; 102(7):2522–2531. [PubMed: 12791667]
39. Rozemuller H, Knaan-Shanzer S, Hagenbeek A, van Bloois L, Storm G, Martens AC. Enhanced engraftment of human cells in RAG2/gammac double-knockout mice after treatment with CL2MDP liposomes. Exp Hematol. 2004; 32(11):1118–1125. [PubMed: 15539091]
40. An Z, Jiang P, Wang X, Moossa AR, Hoffman RM. Development of a high metastatic orthotopic model of human renal cell carcinoma in nude mice: benefits of fragment implantation compared to cell-suspension injection. Clin Exp Metastasis. 1999; 17(3):265–270. [PubMed: 10432012]
41. Zhang XH, Jin X, Malladi S, Zou Y, Wen YH, Brogi E, Smid M, Foekens JA, Massague J. Selection of bone metastasis seeds by mesenchymal signals in the primary tumor stroma. Cell. 2013; 154(5):1060–1073. [PubMed: 23993096]
42. Hoffmann NE, Gillett MD, Cheville JC, Lohse CM, Leibovich BC, Blute ML. Differences in organ system of distant metastasis by renal cell carcinoma subtype. J Urol. 2008; 179(2):474–477. [PubMed: 18076920]
43. Sahi C, Knox JJ, Clemons M, Joshua AM, Broom R. Renal cell carcinoma bone metastases: clinical advances. Ther Adv Med Oncol. 2010; 2(2):75–83. [PubMed: 21789128]

44. Vrdoljak E, Rini B, Schmidinger M, Omrcen T, Torday L, Szczylik C, Sella A. Bisphosphonates and vascular endothelial growth factor-targeted drugs in the treatment of patients with renal cell carcinoma metastatic to bone. Anticancer Drugs. 2013; 24(5):431–440. [PubMed: 23511427]

45. Wood SL, Brown JE. Skeletal metastasis in renal cell carcinoma: current and future management options. Cancer Treat Rev. 2012; 38(4):284–291. [PubMed: 21802857]

46. Vaishampayan U. Cabozantinib as a novel therapy for renal cell carcinoma. Curr Oncol Rep. 2013; 15(2):76–82. [PubMed: 23292795]

47. Pal SK, Quinn DI. Differentiating mTOR inhibitors in renal cell carcinoma. Cancer Treat Rev. 2013; 39(7):709–719. [PubMed: 23433636]

48. Okui T, Shimo T, Fukazawa T, Kurio N, Hassan NM, Honami T, Takaoka M, Naomoto Y, Sasaki A. Antitumor effect of temsirolimus against oral squamous cell carcinoma associated with bone destruction. Mol Cancer Ther. 2010; 9(11):2960–2969. [PubMed: 20858724]

49. Hussein O, Tiedemann K, Murshed M, Komarova SV. Rapamycin inhibits osteolysis and improves survival in a model of experimental bone metastases. Cancer Lett. 2012; 314(2):176–184. [PubMed: 22014409]

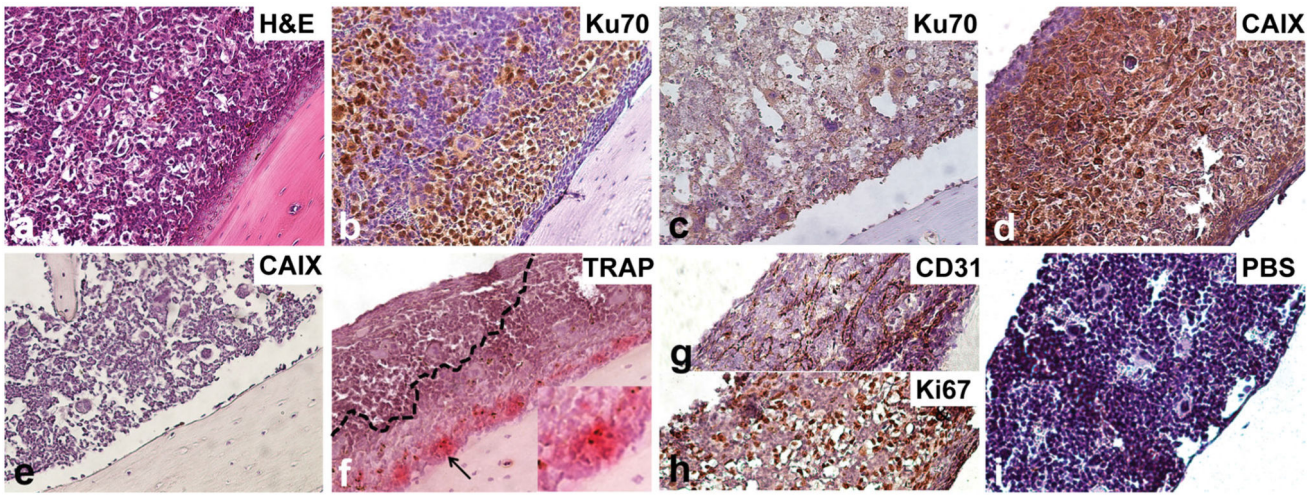

Fig. 1.

Immunophenotype of TSG bone metastases. Bone metastasis in femur of a mouse bearing case 1 TSG at passage 6. Photomicrographs (magnification ×20) showing H&E staining of bone marrow (**a**), immunohistochemistry for Ku70 (**b**) and CAIX (**d**), specific activity of TRAP, indicative of osteoclastic resorption capacity (**f**), and immunohistochemistry for CD31 (**g**), Ki67 (**h**), and negative control (**i**). Control bone stained with Ku70 (**c**) and CAIX (**e**) was negative. Insert in (**f**) shows a ×40 magnification of the area indicated by the black arrow

a

Passage	*Bone micro-metastases*
3	2/6
4	4/5
5	1/1
6	3/4
7	2/2
8	6/6
9	3/3

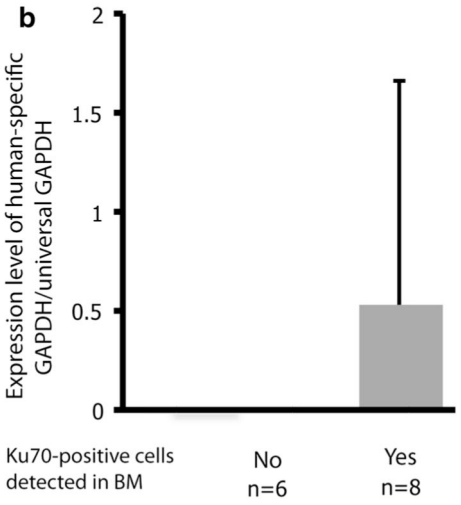

Fig. 2.

Effect of TSG passaging on bone metastasis. a Case 1 TSGs were passaged and bone marrows were analyzed by qRT-PCR for human-specific GAPDH, indicative of metastasis. Bone metastasis showed the number of mice that had bone metastasis/number of mice studied. **b** Bone metastasis (BM) burden (expression level of human-specific GAPDH/ universal GAPDH) was higher if bone metastasis could be confirmed by histology

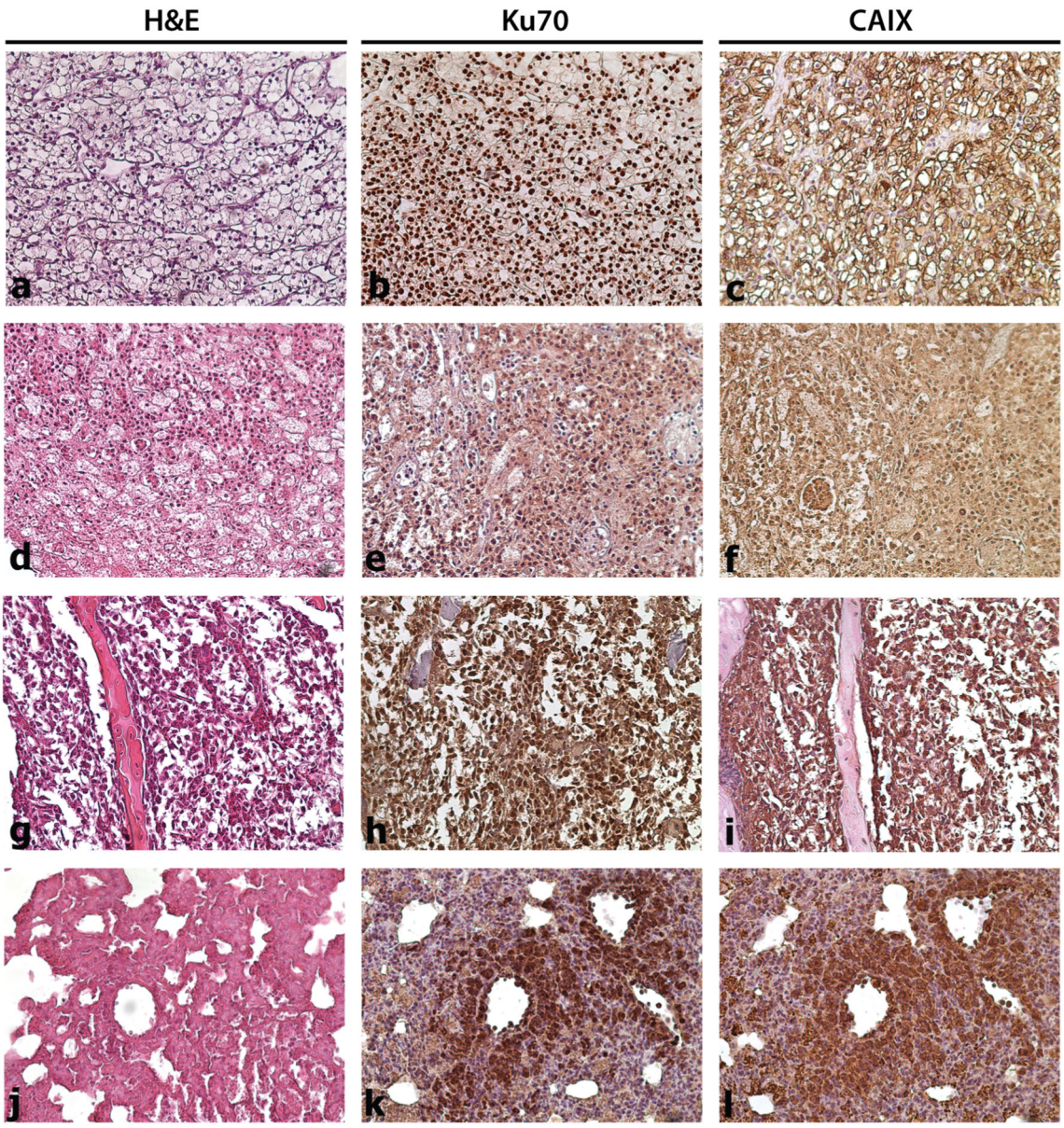

Fig. 3.

Effect of cryopreservation on immunophenotype of TSGs and bone metastasis. TSGs from case 1 at passage 6 were cryopreserved for several weeks and then implanted into mice. **a** H&E-staining of parent tumor of case 1 RCC. **b**, **c** Human-specific Ku70 and CAIX immunohistological stainings of **a**, respectively. **d** H&E-stained passage 6 TSG after cryopreservation showed similar phenotype to parent tumor. **e**, **f** Ku70 and CAIX immunohistological stainings of **d**, respectively. **g** H&E-stained TSG that metastasized to bone after cryopreservation. **h**, **i** Ku70 and CAIX immunohistological stainings of **g**, respectively. **j** H&E-stained TSG that metastasized to lung after cryopreservation. **k**, **l** Ku70 and CAIX immunohistological stainings of **j**, respectively. Magnification is ×20

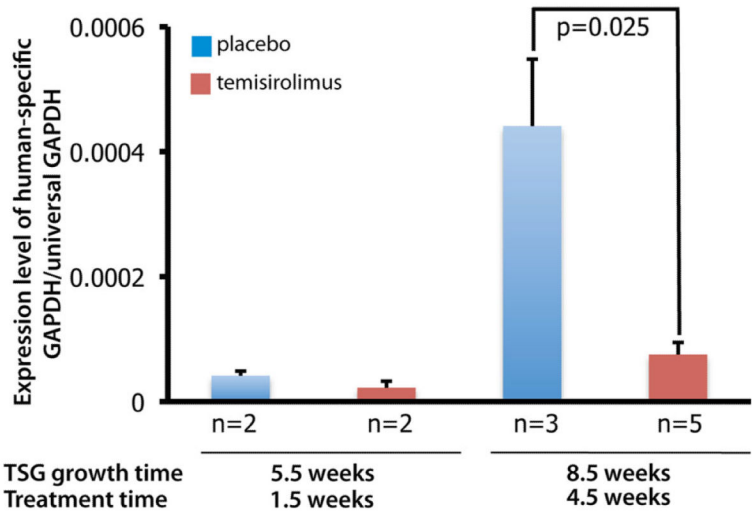

Fig. 4.

Effect of Temsirolimus on bone metastases derived from TSGs. Mice were implanted with passage six TSGs from case 1 and treated with placebo or Temsirolimus at 4 weeks. Bone marrow was analyzed at sacrifice (1.5 and 4.5 weeks after treatment started) for bone metastasis burden. Temsirolimus decreased bone metastasis burden significantly after 4.5-weeks of treatment

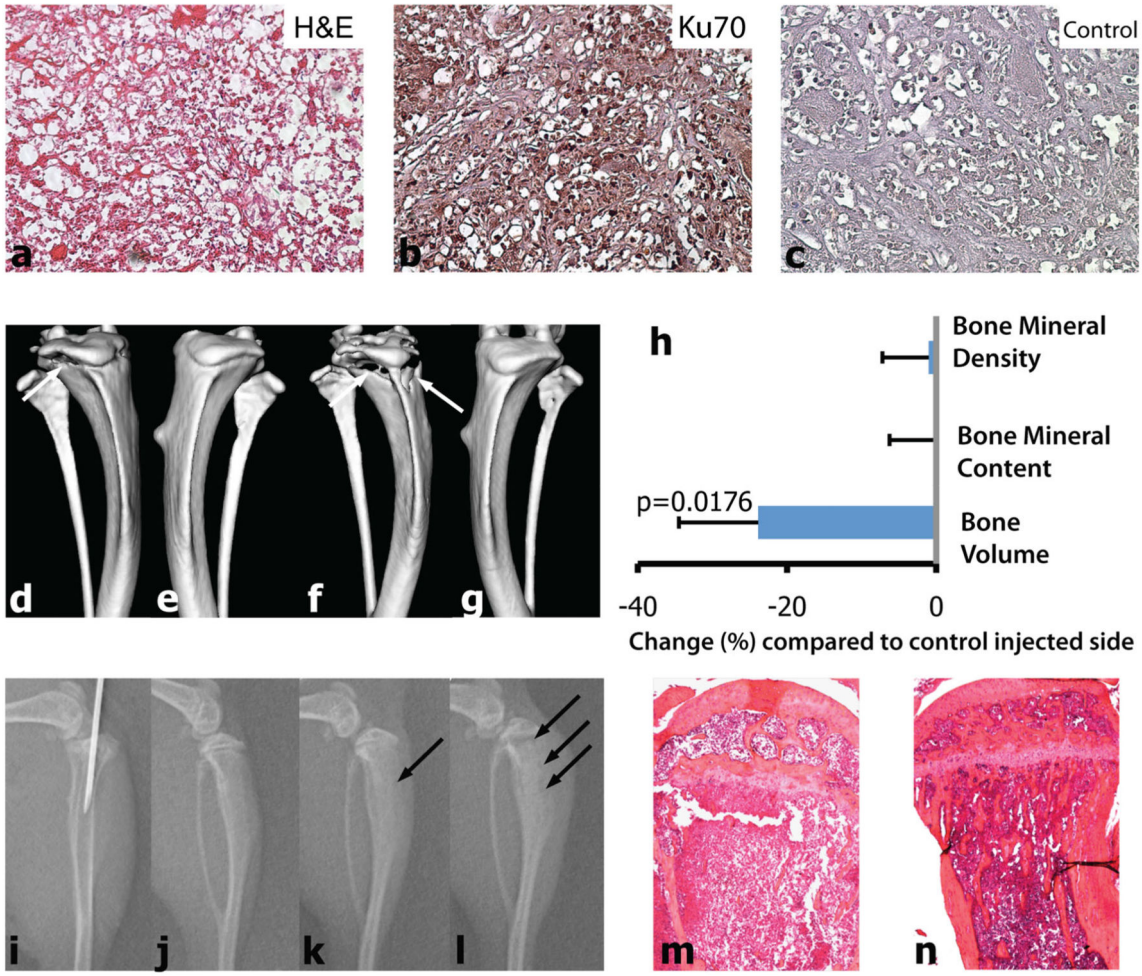

Fig. 5.

Intratibial injection of primary RCC cells results in bone osteolysis in mice. Precision-cut 300 lm thick tissue slices from case 1 TSG at passage six were digested into single cells with collagenase. Histology of frozen sections of precision-cut TSGs confirmed cancer. **a** H&E-staining. **b** Immunohistochemical staining for Ku70. **c** Negative control. The magnification for **a**-**c** is ×20. The correct position of the needle was confirmed with X-ray and single cells were injected into tibiae of mice (**i**). μCT analysis confirmed the advancing lytic appearance of the lesions: tumor-bearing right tibia 4- (**d**) and 6-(**f**) weeks after injection of primary cancer cells; **e** and **g**, corresponding left tibia with no tumor. **h** Volumetric bone analysis with μCT showed reduction in bone volume of the tumor-bearing tibiae at 6 weeks after cancer cell inoculation compared to control injected side (n = 3). Consecutive X-ray images (**j**, day 0, i.e., before injection, and **k** and **l**, 3- and 5-weeks after injection, respectively) revealed development of advancing lytic lesions (arrows in **k** and **l**). **m** H&E-staining of cross-section of tumor cell-injected tibia revealed destruction of trabecular bone and thinning of cortical bone compared to HBS-injected control tibia (**n**). Magnification for **m** and **n** is ×4

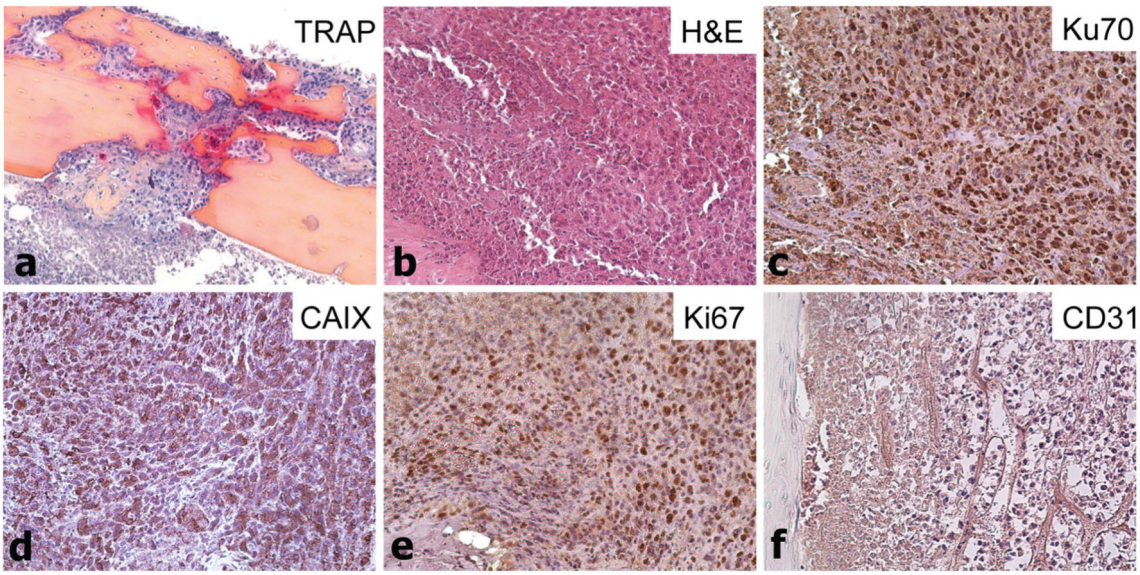

Fig. 6.

Immunophenotype of intratibial tumors derived from single cells. **a** Specific activity of TRAP indicating osteoclastic activity on bone/tumor interface. H&E-staining (**b**), immunohistochemistry for Ku70 (**c**), CAIX (**d**), Ki67 (**e**) and CD31 (**f**) of primary RCC cell-derived intratibial tumors from case 1. Magnification is 20×

Table 1

Pathological features and bone metastasis of RCC cases in this study

Case	Sex	Age	Pathologic Stage	Nodal and Metastatic Stage	Fuhrman Grade	Additional pathologic features	Bone micro-metastasis[a]	Histological verification of bone metastasis[b]	Soft tissue metastasis[c]	Patient outcome at 6 months
1	F	64	T3a	NxMx	III		23/31	8/14	17/31	Metastastic disease (lung, renal, pancreatic)
2	M	75	T2a	NxMx	III/IV	Rhabdoid, papillary	0/4	ns	1/4	Metastatic disease (lung)
3	M	62	T3a	NxMx	III		0/2	ns	0/2	No recurrence
4	M	68	T3a	NxMx	Chromophobe	Papillary	3/4	ns	0/4	Multiple bone metastases
5	M	91	T3a	NxM1	III		0/7	ns	0/7	Not known
6	F	59	T3a	NxM1[d]	IV	Rhabdoid	0/10	0/3	0/10	Not known
7	M	42	T3a	NxMx	III		1/7	0/2	0/7	No recurrence

ns not studied

[a] Bone micrometastasis shows the number of mice that had bone metastasis/number of mice studied, detected by human-specific qRT-PCR

[b] Histological verification of bone metastasis shows the number of mice with histologically confirmed metastasis/mice studied, detected by H&E and human-specific immunohistochemistry (human-specific Ku70 and/or CAIX-staining). In case 1, bones from 18 different TSG-bearing mice were studied and 14 of those were from mice that had bone micrometastases detected by qRT-PCR. Eight metastases of these were confirmed histologically

[c] Soft tissue metastasis shows the number of mice that had soft tissue metastasis (liver or lung)/number of mice studied at sacrifice

[d] This patient underwent surgical removal of brain and bone metastases, followed by two cycles of Sunitinib, prior to nephrectomy and implantation of tissue into mice

Clin Exp Metastasis. Author manuscript; available in PMC 2015 March 06.

Table 2

Effect of cryopreservation on TSG engraftment and metastasis

Experiment	Cryopreserved TSG	Average graft size (mg) ± SD	Engraftment rate (engrafted/total)	Bone micro-metastasis[a]	Histological verification of bone metastasis[b]	Soft tissue metastasis[c]	Liver Lung
1	Case 1 passage 8	1,573 ± 350	9/9	2/2	1/1	9/9	1/9
2	Case 1 passage 9[d]	676.33 ± 517	4/5	ns	1/2	1/3	1/3
3	Case 1 passage 10	1,426 ± 357	3/5	ns	1/2	2/3	2/3

ns not studied

[a] Bone micrometastasis shows the number of TSG-bearing mice that had bone metastasis/number of mice studied, detected by human-specific qRT-PCR

[b] Histological verification of bone metastasis shows number of mice with histologically confirmed metastasis/mice studied, detected by H&E and human-specific IHC

[c] Soft tissue metastasis shows the number of mice that had soft tissue metastasis/number of mice studied at sacrifice. For experiment 2 and 3, the same mice had both liver and lung metastases

[d] In experiment 2, minced tissue (smaller than 1 mm^3) was used instead of slices

Table 3

Intratibial bone metastasis model

Experiment	TSG	Engraftment rate (engrafted/total)	Osteolysis rate (osteolysis confirmed by μCT/total)
1	Case 1 passage 6	5/5	5/5
2	Case 1 passage 8[a]	5/5	5/5

[a] Single cells derived from TSG were cryopreserved and thawed prior to inoculation into tibiae of mice